Dynamic Modeling and Transient Analysis of a 5 × 5 Node Array in Solid Oxide Electrolysis Cell Using Quasi-3D Approach

Jiwon Ahn [a], Hyoung Kyu Cho [a*], Byung Ha Park [b], Chan-Soo Kim [b]
[a] *Department of Nuclear Eng., Seoul National Univ., 1 Gwanak-ro, Gwanak-gu, Seoul 08826*
[b] *Nuclear Hydrogen Research Team, Korea Atomic Energy Research Institute, 111 Daedeok-daero 989 beon-gil, Yuseong-gu, Daejeon 34057*
**Corresponding author: chohk@snu.ac.kr*

1. Introduction

Hydrogen demand has increased continuously, and it is expanding as an energy carrier. Among various feasible hydrogen production methods, the solid oxide electrolysis cell (SOEC) is one of the promising technologies due to its lower required electricity resulting from high-temperature steam usage than other methods. Simultaneously, SOEC has technical issues such as sealing and thermal cycling which cause cell damage in Sohal et al. [1]. In connection with the issues, some studies have been conducted to predict the temperature fields in the SOEC cell. Xiaodong et al.'s work [2] is one of the leading studies for a SOEC temperature estimator.

As the first step to estimating the temperature distribution in a SOEC cell accurately and efficiently, this study proposed a simple quasi-3D (1D + 2D) model developed using MATLAB Simulink®. A 5 × 5 node array in a SOEC cell was analyzed and the results were compared with available experimental data in Momma et al. [3] for the model validation. In addition, the temperature distribution of the SOEC cell center obtained from the model and efficiency of SOEC were presented and discussed.

2. Model descriptions

Fig. 1 depicts the SOEC model considered in the present study. It consists of a 5×5 node array, which is the number compromised by Mahshid et al. [4]. Each node contains seven control volumes and three sub-models. The seven control volumes are determined by the physical structure of the SOEC cell illustrated in the right figure of Fig. 1. The three sub-models include the electrochemical model, species conservation, and energy balance to observe the transient behavior of the SOEC cell.

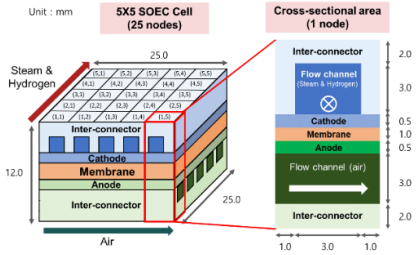

Fig. 1. The schematic diagram of a cross-flow SOEC cell divided into 5×5 nodes and 7 control volumes for models.

2.1. Electrochemical model

The electrochemical model is used to calculate the electrical energy input and determines the operation mode; when the operating voltage is over the thermo-neutral voltage (V_{th}), the SOEC cell release heat after the reaction (Fig. 2). In the other case, the SOEC cell absorbs the heat from the overvoltages and outside to decompose water.

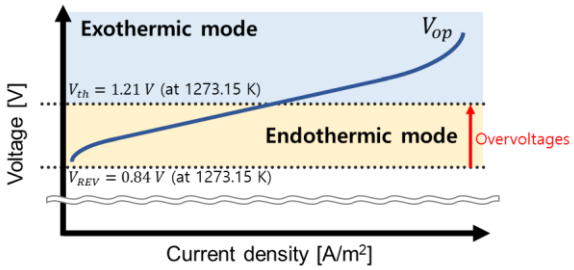

Fig. 2. Operation modes of SOEC.

The operating voltage can be expressed as a sum of reversible voltage and overvoltages:

$$V_{Op} = V_{REV} + V_{act,an} + V_{act,cat} + V_{ohmic} + V_{con} \quad (1)$$

where V_{Op} is the operating voltage of the cell; V_{REV} is the reversible voltage; $V_{act,an}$ and $V_{act,cat}$ are the activation overvoltages at the anodic and cathodic sides, respectively; V_{ohmic} is the ohmic overvoltage; V_{con} is the concentration overvoltage. The elements of V_{Op} are dominated by temperature.

The operating voltage is determined by the current density. After the power is put into the cell, hydrogen evaluation reaction (HER) occurs through the water splits at the cathodic triple-phase boundary (TPB). TPB is a region between three phases: reactants, electrolyte (membrane), and electrode. The time scale of the electrochemical reaction is on the order of 0.001 seconds [13]. Therefore, the dynamics of electrochemical reaction such as charge/discharge process for electric double-layer can be negligible [14].

2.2. Species conservation

For the electrochemical reaction, the reactants have to be supplied to the catalyst layer and the products have to be discharged continuously by the mass transfer phenomena. The driving mechanisms of the transfer are the diffusion by the concentration difference between both sides of the electrodes and the working fluid. As a result of the reaction, the composition of species changes. The following equation infers the changes in the species concentrations.

$$\frac{d(N_{avg}X)}{dt} = \dot{N}_{in}X_{in} - \dot{N}_{out}X_{out} + \sum \overrightarrow{\Phi} \quad (2)$$

where N, $\dot{N}$ and X are total mole number in the control volume, molar flowrate and mole fraction of species; $\overrightarrow{\Phi}$ is species' molar flowrate by diffusion phenomena. The diffusion flowrate is calculated as:

$$\overrightarrow{\Phi}_i = D^{eff}\nabla C_i \quad (3)$$

where D^{eff} is effective diffusion coefficient of the porous electrode; C is molar concentration of the species; the subscript i is a sort of species.

2.3. Energy conservation

Energy conservation is used to determine the temperature of the control volumes. After the electrochemical reaction, heat adsorbs or emits depending on the energy supplied to decompose water. The following equation connotes the transient behaviors of each control volume.

$$\left(\sum \rho V C_p\right)\frac{dT}{dt} = \dot{N}_{in}h_{in} - \dot{N}_{out}h_{out} + \dot{Q}_{net} \quad (4)$$

where ρ, V, and C_p are density, volume, and heat capacity, respectively; h is molar average molar enthalpy of species; $\dot{Q}_{net}$ is the net heat transfer rate by conduction and convection to the control volume. In the membrane, $\dot{Q}_{net}$ includes the heat by the electrochemical reaction. Table 1 shows the parameters used to obtain the heat transfer rate in each control volume.

Table 1. Heat transfer parameters of the SOEC cell.

Control volume	Thermal conductivity [W/m·K]	Nusselt number [-]
Membrane	2 [5]	
Anode	4 [5]	
Cathode	2 [6]	
Flow channel (both sides)		3.09 [7, 8]
Inter-connector (both sides)	20 [9]	

3. Result

The quasi-3D SOEC model for the 5×5 node array was developed in MATLAB Simulink®. Before simulating the developed model, the model was validated by comparing it with the experimental data. Using the validated model, the transient behavior of the SOEC cell center was investigated under endothermic and exothermic operation modes. Moreover, the efficiency and the amount of the produced hydrogen and the efficiency to produce hydrogen in each operation mode were contemplated. The operating conditions of the two cases are shown in Table 2.

Table 2. Operating conditions of the SOEC cell.

Operating Condition		Endothermic	Exothermic
Initial current density [A/m²]		2000	4000
Inlet conditions		**Cathode**	**Anode**
Temperature [K]		1273.15	1273.15
Pressure [bar]		1	1
Ratio	H_2/H_2O	0.4/0.6	
	O_2/N_2		0.21/0.79

3.1. Validation

The data used for the validation were reported in Ref. [3]. It was an experiment under steady-state. As shown in Fig. 3, the model follows the experimental data well overall, with an average error of 2.81 % and a maximum error of 6.26 % except for near zero current density conditions. The discrepancy near zero current density can be inferred that the actual reaction occurs above the reversible voltage.

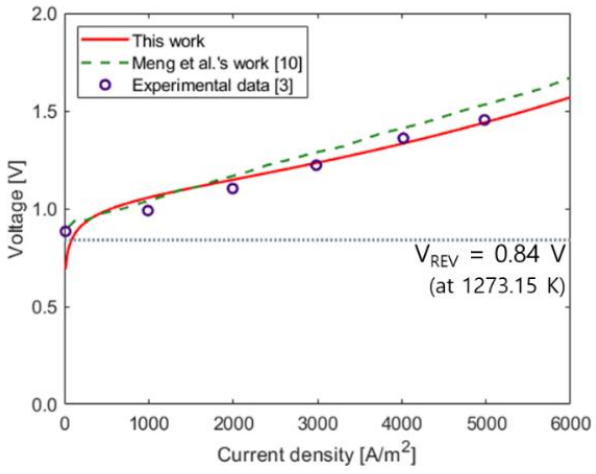

Fig. 3. Comparison of the model and experimental data.

3.2. Endothermic condition

This section analyzed the temperature changes in the center of the SOEC cell in the endothermic operation. In the mode, the electrochemical reaction consumes the energy continuously, therefore, the temperature of the control volumes decreases over time (Fig. 4). In addition, the temperature of the control volumes rapidly decreases within initial 100 seconds after the start-up. Furthermore, the temperatures reach the steady-state at about 1000 seconds, which implies that the heat transfer rates by the temperature difference between the control volumes become constant over 1000 seconds.

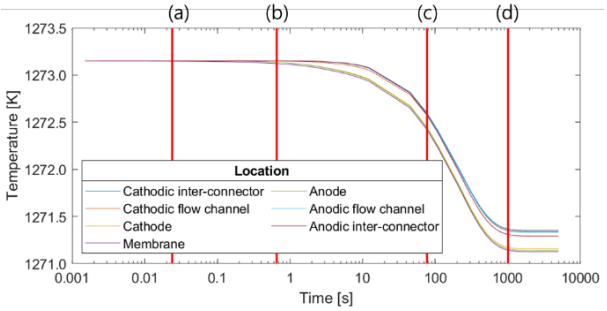

Fig. 4. Transient temperatures of each control volume in the endothermic operation mode.

Fig. 5 displays the temperature distribution at four time steps in the transient analysis. When the SOEC cell begins to operate (Fig. 5-a), the membrane temperature initially drops sharply, and its effect spreads to all the control volumes in the cell. The temperature of the flow channel seems to be higher than surroundings due to the low thermal conductivity of the gas in the flow channel. The temperature drop of the inter-connectors causes temperature difference between the inter-connectors and the outside where maintains a constant temperature (1273.15 K), which transfers heat from outside to the inter-connectors. Therefore, the temperature of the inter-connector decreases more slowly than the flow channel. As a result, the temperature difference between the flow channel and the inter-connector disappears at t=0.65 sec (Fig. 5-b). The temperature of the electrodes on both sides of the membrane and the gas in the flow channels decreases continuously according to the consecutive endothermic electrochemical reaction as shown in Fig. 5-c. The temperature of the anode is lower than that of the cathode because the thermal conductivity of the anode is more significant than that of the cathode. In the steady state, the temperature of the solid element on the anodic side is lower than that on the cathodic side in the steady-state because of the high thermal conductivity of anode (Fig.5-d).

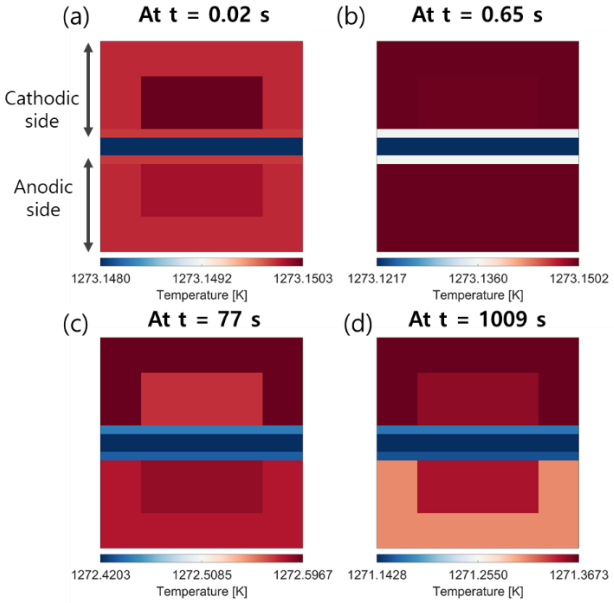

Fig. 5. Temperature relationship between each control volume of the cross-sectional area at the center of the SOEC cell in endothermic operation mode at (a) t = 0.02 s, (b) t = 0.65 s, (c) t = 77 s, (d) t = 1009 s.

3.3. Exothermic condition

The exothermic reaction occurs when more energy than required to split water is supplied. The surplus energy is released as the thermal energy. Therefore, the consecutive exothermic electrochemical reaction leads to heat up the SOEC cell until the heat balance between the control volume composed of the SEOC cell is achieved. Under Fig. 6, the temperature of the cell increases over 1000s and reaches a steady state.

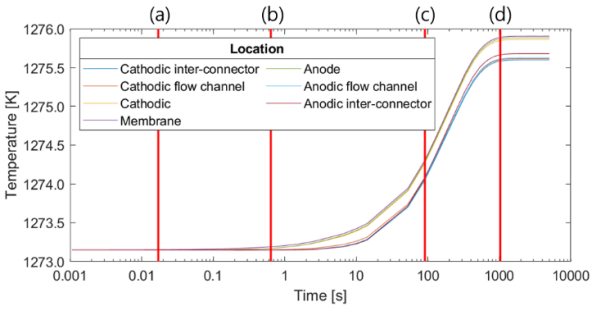

Fig. 6. Transient temperatures of each control volume over time in the exothermic operation mode.

Fig. 7 shows the transient temperature relationship for each control volume of the cross-sectional area of the cell center in the exothermic operation. Immediately after the operation, the membrane first heats up, and the effect diffuses to the solid-state electrodes and inter-connectors remarkably. Furthermore, the effect on the flow channel in which gas exists appears about 0.63 seconds after the operation so that the interface between the flow channel and the inter-connector becomes

indistinguishable. Then, because of the heat transfer from the inter-connectors to the outside, the boundary between the flow channel and the inter-connector becomes clear about 14 seconds after the operation. At 1009 seconds, the steady-state temperature distribution can be obtained. For the same reason as the endothermic operation mode, the anodic electrode and the inter-connector temperatures are higher than those of the cathodic electrode and the inter-connector.

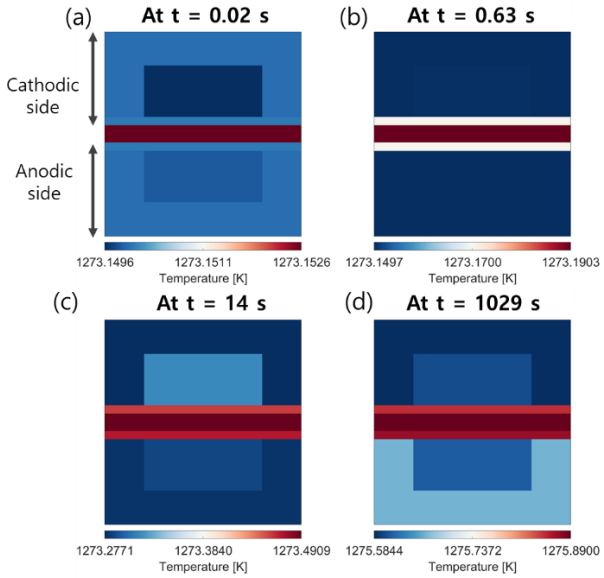

Fig. 7. Temperature relationship between each control volume of the cross-sectional area at the center of the SOEC cell in exothermic operation mode at (a) t = 0.02 s, (b) t = 0.63 s, (c) t = 14 s, (d) t = 1029 s.

3.4. Hydrogen production

Summarizing the transient behaviors under the two operation modes, the membrane temperature decreased 2 K (0.15 % of the initial temperature) over 1009 seconds in the endothermic operation mode and increased 2.5 K (0.2 % of the initial temperature) over 1029 seconds in the exothermic operation mode. The tiny temperature changes attribute to the small size of the SOEC cell used to modeling, which suggests the size of the SOEC cell can be enlarged. Besides, as the electrochemical reaction occurs on the membrane surface, the current densities in all the nodes can be assumed to be constant.

From the assumption, the amount and the efficiency of the produced hydrogen can be calculated by Eq. (5) and Eq. (6), respectively.

$$\dot{n}_{H_2} = \frac{I}{2F} \tag{5}$$

where $\dot{n}_{H_2}$ is molar flowrate of the produced hydrogen; I is the current which can be expressed as a multiple of the active area and the current; F is Faraday constant (96 485 C/mol) [10].

To calculate the thermal efficiency, faradaic efficiency is considered equal to 1. The thermal efficiency can be represented by Ref. [11, 12]:

$$\eta = \frac{\dot{n}_{H_2} \times LHV_{H_2}}{IV_{op} + Q_{in}} \times 100\ (\%) \tag{6}$$

where LHV_{H_2} is lower heating value of hydrogen; Q_{in} is the heat input to split water in the endothermic mode.

Under the conditions of Table. 2, the amount of hydrogen is 0.52 Nm^3/hr and 1.04 Nm^3/hr in the endothermic and exothermic mode respectively. And the electricity demand to produce hydrogen is 32.08 kWh/kg and 39.34 kWh/kg in the endothermic and exothermic mode respectively. The thermal efficiency of hydrogen production is 100 % and 88.02 % in the endothermic and exothermic mode respectively. The efficiency in the endothermic operation indicates the heat has to absorb to react and be supplied from the surrounding such as gas in the flow channels.

4. Conclusion

This study developed a quasi-3D SOEC model and validated the model with experimental data. The transient behavior of the cross-sectional area temperature in the center of the SOEC cell and the efficiency of hydrogen production were investigated under endothermic and exothermic operation mode. Furthermore, effects of the two operation modes on hydrogen were envisaged. In future work, this study will investigate the precise transient behavior of SOEC cells by expanding the number of nodes and increasing the number of control volumes. In addition, this model will be extended to simulating the green hydrogen production system by connecting with other components of a nuclear power plant.

Acknowledgements

This study was supported by Nuclear Research and Development Program (2021M2D4A204677) of the National Research Foundation of Korea (NRF) grand funded by the Korean Government (MSIP).

REFERENCES

[1] Sohal, M. S., J. E. O'Brien, C. M. Stoots, V. I. Sharma, B. Yildiz, and A. Virkar. Degradation Issues in Solid Oxide Cells During High Temperature Electrolysis, Proceedings of the ASME 2010 Eighth International Fuel Cell Science, Engineering and Technology Conference FuelCell2010, June 14-16, 2010, Brooklyn, New York, USA.
[2] Xiaodong Wu, Jianhua Jiang, Weiqi Zhao, Xi Li, Two-dimensional temperature distribution estimation for a cross-flow planar solid oxide fuel cell stack, International Journal of Hydrogen Energy, Vol. 45, Issue 3, pp.2257-2278, 2020.
[3] Momma A, Kato T, Kaga Y, Nagata S, Polarization behavior of high temperature solid oxide electrolysis cells (SOEC), Journal of the Ceramic Society of Japan, Vol. 105, Issue 5, pp.369-373, 1997.

[4] Mahshid Fardadi, Fabian Mueller, Faryar Jabbari, Feedback control of solid oxide fuel cell spatial temperature variation, Journal of Power Sources, Vol. 195, Issue 13, pp.4222-4233, 2010.
[5] Zonglei Xu, Xiongwen Zhang, Guojun Li, Guoping Xiao, Jian-Qiang Wang, Comparative performance investigation of different gas flow configurations for a planar solid oxide electrolyzer cell, International Journal of Hydrogen Energy, Vol. 42, Issue 16, pp.10785-10801, 2017.
[6] Marko Nerat, Đani Juričić, A comprehensive 3-D modeling of a single planar solid oxide fuel cell, International Journal of Hydrogen Energy, Vol. 41, Issue 5, pp.3613-3627, 2016.
[7] Q. Cai,E. Luna-Ortiz,C. S. Adjiman,N. P. Brandon, The Effects of Operating Conditions on the Performance of a Solid Oxide Steam Electrolyser: A Model-Based Study, Fuel Cells, Vol. 10, Issue 6, pp.1114-1128, 2010.
[8] P. Aguiar, C.S. Adjiman, N.P. Brandon, Anode-supported intermediate temperature direct internal reforming solid oxide fuel cell. I: model-based steady-state performance, Journal of Power Sources, Vol. 138, Issues 1–2, pp.120-136, 2004.
[9] David L. Damm, Andrei G. Fedorov, Reduced-order transient thermal modeling for SOFC heating and cooling, Journal of Power Sources, Vol. 159, Issue 2, pp.956-967, 2006.
[10] Meng Ni, Michael K.H. Leung, Dennis Y.C. Leung, Parametric study of solid oxide steam electrolyzer for hydrogen production, International Journal of Hydrogen Energy, Vol. 32, Issue 13, pp. 2305-2313, 2007.
[11] Mithila N. Manage, Eva Sorensen, Stefaan Simons, Dan J.L. Brett, A modelling approach to assessing the feasibility of the integration of power stations with steam electrolysers, Chemical Engineering Research and Design, Vol. 92, Issue 10, pp. 1988-2005, 2014.
[12] Günter Schiller, Michael Lang, Patric Szabo, Nathalie Monnerie, Henrik von Storch, Jan Reinhold, Pradeepkumar Sundarraj, Solar heat integrated solid oxide steam electrolysis for highly efficient hydrogen production, Journal of Power Sources, Vol. 416, pp. 72-78, 2019.
[13] Ryan O'Hayre PhD, Suk-Won Cha PhD, Whitney Colella PhD, Fritz B. Prinz PhD, Fuel Cell Fundamentals, John Wiley & Sons., pp. 77-116, 2016.
[14] Yun Wang, Chao-Yang Wang, Transient analysis of polymer electrolyte fuel cells, Electrochimica Acta, Vol. 50, Issue 6, pp. 1307-1315, 2005.